ISSN 1070-3284, Russian Journal of Coordination Chemistry, 2014, Vol. 40, No. 4, pp. 251–256. © Pleiades Publishing, Ltd., 2014.

Synthesis, Crystal Structure, and Properties of a New Lanthanide Tartrate Coordination Polymer[1]

W. Xu, H. S. Chang, W. Liu, and Y. Q. Zheng*

Center of Applied Solid State Chemistry Research Ningbo University, Ningbo, 315211 P.R. China

**e-mail: yqzhengmc@163.com*

Received January 1, 2013

Abstract—A new coordination polymer of terbium tartrate $[Tb(H_2O)_3(C_4H_5O_6)(C_4H_4O_6)]$ has been synthesized and crystallizes in the polar space group $P4_1$ with cell constants $a = 6.0415(9)$, $b = 6.0415(9)$, $c = 36.516(7)$ Å, $V = 1332.8(4)$ Å^3, $Z = 4$. The terbium(III) ion of title complex is nine-coordinate through oxygen donors. Four different coordination modes of tartrate occur. This Tb(III) complex exhibits a characteristic luminescence in the visible region upon excitation at 353 nm. The temperature-dependent magnetic properties of the Tb(III) complex were investigated in the temperature range of 2–300 K. Title compound exhibits significant ferroelectric properties at room temperature (remnant polarization $2P_r = 0.160$ μC cm^{-2}, coercive field $2E_c = 44.5$ kV cm^{-1}, saturation of the spontaneous polarization $P_s = 0.176$ μC cm^{-2}).

DOI: 10.1134/S1070328414030105

INTRODUCTON

Compounds of several tartrates have very interesting physical properties including ferroelectricity, piezoelectricity and optical second harmonic generation [1–7]. Consequently, they are used in transducers and several linear and nonlinear mechanical devices. This has led many investigators to grow single crystals of tartrate compounds and study their characteristics [8–11]. The rare earth metals have many important properties such as exhibiting a high coordination number, strong magnetism, fluorescence, neutron aborption and catalysis [12–14]. The design and synthesis of lanthanide tartrates have attracted many of workers interesting. Although single crystal X-ray structure analyses of several lanthanide tartrates have been reported, almost all of the reports were focused on the syntheses and crystal structures, the information on physicochemical properties of lanthanide tartrate is limited. Magnetic properties of gadolinium tartrates [15] were discussed by Chaudhuri and co-workers. Nitrogen adsorption behaviors were observed lanthanum tartrate, cerium tartrate and praseodymium tartrate [16]. Lanthanide tartrates include europium, terbium, and dysprosium [17] have investigated luminescent properties.

In this paper, a terbium tartrate coordination polymer $[Tb(H_2O)_3(C_4H_5O_6)(C_4H_4O_6)]$ (**I**) has been obtained by reaction of tartaric acid and terbium chloride. X-ray crystallographic analysis reveals that it belongs $P4_1$ space group, also indicates space group by powder X-ray diffraction. Low-temperature magnetic susceptibility measurements show weak antiferromagnetic interaction between the terbium ions. What's more, here exists an electric hysteresis loop that is a typical ferroelectric feature.

EXPERIMENTAL

Materials and physical methods. All chemicals of reagent grade were commercially available and used without further purification. Powder X-ray diffraction measurements were carried out with a Bruker D8 Focus X-ray diffractometer to check the phase purity. Single-crystal X-ray diffraction data were collected on a Rigaku R-Axis Rapid X-ray diffractometer. The C, H, and N microanalyses were performed with a PE 2400II CHNS elemental analyzer. The FT-IR spectrum was recorded from KBr pellets in the range 4000–400 cm^{-1} on a Shimadzu FTIR-8900 spectrometer. Fluorescence emission spectra were recorded in the solid state on HITACHI F-4600 fluorescence spectrophotometer. The temperature-dependent magnetic susceptibility was determined with a Quantum Design SQUID magnetomer (Quantum Design Model MPMS-7) in the temperature range 2–300 K with an applied field of 5 kOe. The ferroelectric property of the solid-state sample was measured by a pellet of powdered sample using a Premier station ferroelectric tester at room temperature while the sample was immerged in insulating oil.

Synthesis of I. The pH of a mixture of $TbCl_3$ prepared from Tb_4O_7 (0.149 g, 0.2 mmol) dissolved in 5 mL diluted HCl and L-(+)-tartaric acid (0.06 g, 0.4 mmol) in 30 mL H_2O was adjusted to 2.65 with diluted HCl under stirring. Colorless crystals of the title compound

---

[1] The article is published in the original.

Table 1. Crystallographic data and refinement details for **I**

Parameter	Value
Formula weight	510.12
Crystal habit; color	Block; colorless
Crystal system	Tetragonal
Space group	$P4_1$
T, K	293(2)
a, Å	6.0415(9)
c, Å	36.516(7)
Volume, Å	1332.8(4)
Z	4
ρ_{calcd}, g cm^{-3}	2.542
μ, mm^{-1}	5.399
F(000)	992
θ Range for data collection, deg	3.37–27.46
Reflections collected	12831
Independent reflections (R_{int})	3041 (0.0504)
Reflection with $I \geq 2\sigma(I)$	2861
Number of parameters	217
Goodness-of-fit on F^2	1.194
Final R indices ($I \geq 2\sigma(I)$)	0.0276, 0.0300
R indices (all data)	0.0642, 0.0650
Largest difference peak and hole, e Å^{-3}	0.900, –1.482

were obtained after 2 days at a temperature of 45°C. The yield was 154.7 mg (54.6%) based on the initial Tb_4O_7 input.

For $C_8H_{15}O_{15}Tb$		
anal. calcd., %:	C, 18.82;	H, 2.94.
Found, %:	C, 18.76;	H, 3.02.

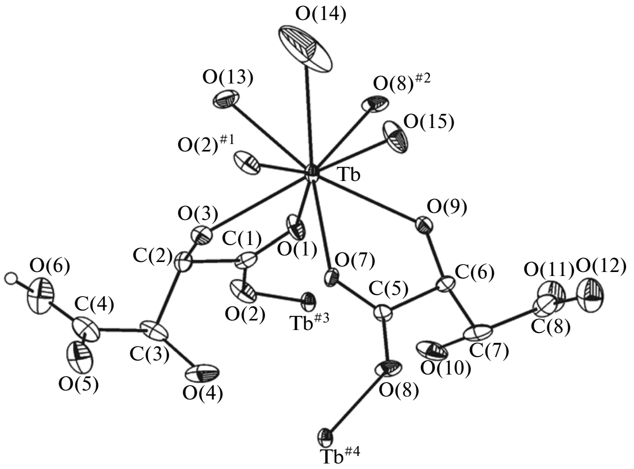

Fig. 1. ORTEP view of the polymer of complex **I**. The displacement ellipsoids are drawn at 45% probability level, hydrogen atoms are omitted for clarity.

IR (KBr; ν, cm^{-1}): 3261 m, 2665 m, 1718 s, 1585 v.s, 1401 s, 1140 s, 1068 s, 941 w, 832 w, 791 m, 682 m, 571 w.

X-ray crystallography. A suitable single crystal of **I** was selected under a polarization microscope and fixed with epoxy cement on a fine glass fiber which was then mounted on a Rigaku R-Axis Rapid IP X-ray diffractometer, operating with graphite-monochromated MoK_α radiation ($\lambda = 0.71073$ Å) for cell determination and subsequent data collection. The data were corrected for Lp and empirical absorption effects. The SHELXS-97 and SHELXL-97 programs were used for structure solution and refinement [18]. The structure was solved by using direct methods. Subsequent difference Fourier syntheses enabled all non-hydrogen atoms to be located. After several refinement cycles, the hydrogen atoms associated with carbon atoms were geometrically generated, and the remainder of the hydrogen atoms were located from successive difference Fourier syntheses. Finally, all non-hydrogen atoms were refined with anisotropic displacement parameters by a full-matrix least-squares technique, and hydrogen atoms with isotropic displacement parameters were set to 1.2 times the values for the associated heavier atoms. Detailed information about the crystal data and structure determination is summarized in Table 1. Selected interatomic distances and bond angles are listed in Table 2.

RESULTS AND DISCUSSION

Compound (Fig. 1) comprises 2D chiral sheets built up by connecting Tb^{3+} ions with bridging *syn-anti* carboxylate groups of tartrates. Each Tb^{3+} ion is nine-coordinate from three oxygens from three waters and six oxygens from four tartates in a tricapped trigonal prism coordination geometry. The bond lengths of Tb–O are in the range of 2.323(5)–2.702(11) Å (Table 2). For the tartrate ligand, each one bridges two Tb^{3+} ions through "1,2-chelation" involving a carboxylate oxygen and the *ortho*-hydroxy with five-membered rings. The carboxylate group O(1) atom and the hydroxyl O(3) atom chelate a Tb atom. Atom O(2) bridges to a aymmetry-related Tb atom, forming a 1D chain along [100] (Fig. 2). In the same way, O(7) and O(9) chelate Tb atom, O(8) bridges another Tb atom between chains, generating 2D layer parallel to the plane (001) (Fig. 3). The layers are linked together through a complicated hydrogen-bonding scheme involving the water ligands, hydroxyl O atoms and the carboxylate O atoms. Thus, a three-dimensional framework is produced (Fig. 4).

Single crystal XRD results also confirm that the material grown in the present investigation is similar to samarium tartrate trihydrate [19], erbium ditartrate trihydrate [20]. Due to complex **I** is terbium(III) ditartrate trihydrate $[Tb(H_2O)_3(C_4H_5O_6)(C_4H_4O_6)]$, and asymmetric unit contains two absolute independence two tartrate of one tartrate anion and one hydrogen-

Table 2. Selected bond lengths (Å) and bond angles (deg) for **I***

Bond	*d*, Å	Bond	*d*, Å	Bond	*d*, Å
Tb–O(1)	2.333(5)	Tb–O(7)	2.323(5)	Tb–O(13)	2.396(7)
Tb–O(2)$^{\#1}$	2.344(5)	Tb–O(8)$^{\#2}$	2.344(5)	Tb–O(14)	2.702(11)
Tb–O(3)	2.503(11)	Tb–O(9)	2.522(12)	Tb–O(15)	2.420(7)
Angle	ω, deg	Angle	ω, deg	Angle	ω, deg
O(1)TbO(2)$^{\#1}$	133.7(2)	O(2)$^{\#1}$TbO(13)	80.6(2)	O(7)TbO(14)	137.0(3)
O(1)TbO(3)	63.7(2)	O(2)$^{\#1}$TbO(14)	69.0(3)	O(7)TbO(15)	85.8(2)
O(1)TbO(7)	85.2(2)	O(2)$^{\#1}$TbO(15)	77.9(2)	O(8)$^{\#2}$TbO(9)	70.3(2)
O(1)TbO(8)$^{\#2}$	81.9(2)	O(3)TbO(7)	73.7(2)	O(8)$^{\#2}$TbO(13)	77.5(2)
O(1)TbO(9)	73.5(2)	O(3)TbO(8)$^{\#2}$	134.9(2)	O(8)$^{\#2}$TbO(14)	67.3(3)
O(1)TbO(13)	86.0(2)	O(3)TbO(9)	121.0(1)	O(8)$^{\#2}$TbO(15)	80.4(2)
O(1)TbO(14)	137.8(3)	O(3)TbO(13)	72.2(3)	O(9)TbO(13)	143.7(2)
O(1)TbO(15)	144.9(2)	O(3)TbO(14)	120.7(4)	O(9)TbO(14)	118.3(4)
O(2)$^{\#1}$TbO(3)	70.0(2)	O(3)TbO(15)	143.9(2)	O(9)TbO(15)	72.1(3)
O(2)$^{\#1}$TbO(7)	81.4(2)	O(7)TbO(8)$^{\#2}$	134.1(2)	O(13)TbO(14)	60.4(4)
O(2)$^{\#1}$TbO(8)$^{\#2}$	136.3(2)	O(7)TbO(9)	63.7(2)	O(13)TbO(15)	118.9(2)
O(2)$^{\#1}$TbO(9)	134.9(2)	O(7)TbO(13)	145.2(2)	O(14)TbO(15)	58.5(4)

O–H···O	Distances, Å			O–H···O angle, deg
	H–O	O···H	O···O	
O(3)–H(3*B*)···O(11)$^{\#3}$	0.86	1.81	2.663(9)	171
O(4)–H(4*B*)···O(12)$^{\#4}$	0.89	2.00	2.857(9)	164
O(6)–H(6)···O(15)$^{\#5}$	0.83	1.81	2.622(9)	168
O(9)–H(9*B*)···O(5)$^{\#6}$	0.86	1.81	2.662(9)	174
O(10)–H(10*B*)···O(6)$^{\#7}$	0.85	2.09	2.863(9)	151
O(13)–H(13*A*)···O(7)$^{\#2}$	0.86	1.89	2.718(8)	161
O(13)–H(13*B*)···O(4)$^{\#2}$	0.86	1.94	2.771(9)	165
O(14)–H(14*A*)···O(4)$^{\#8}$	0.85	2.14	2.950(9)	159
O(14)–H(14*B*)···O(10)$^{\#8}$	0.85	2.05	2.855(9)	158
O(15)–H(15*A*)···O(10)$^{\#1}$	0.84	1.98	2.764(8)	154
O(15)–H(15*B*)···O(1)$^{\#1}$	0.85	1.91	2.708(8)	156

* Symmetry transformations used to generate equivalent atoms: $^{\#1}$ $x, y + 1, z$; $^{\#2}$ $x + 1, y, z$; $^{\#3}$ $y + 1, -x + 1, z - 1/4$; $^{\#4}$ $y, -x, z - 1/4$; $^{\#5}$ $y, -x + 1, z - 1/4$; $^{\#6}$ $-y + 1, x, z + 1/4$; $^{\#7}$ $-y, x - 1, z + 1/4$; $^{\#8}$ $x + 1, y + 1, z$.

tartrate. The one hydrogen-tartrate has one hydrion. There is select space group $P4_1$ with greater accuracy. Further, the phase purity of the crystalline product was confirmed by comparing an experimental powder X-ray diffraction (PXRD) pattern with the corresponding the simulated PXRD on the basis of the single crystal data according to $P4_1$.

The infrared spectrum in the range 400–4000 cm^{-1} shows a wide strong broad band centered at 3261 cm^{-1} due to OH stretching vibration of water and carboxylic acid group. The strong absorptions at 1718 cm^{-1} is attributed to stretching vibration of (COO) bonds, which shows the presence of unionized carboxyl groups in the compound. The strong sharp absorptions at 1585 cm^{-1} result from antisymmetric stretching (ν_{as}) of the carboxylate groups, and symmetric stretching (ν_s) of the carboxylate groups cause strong sharp absorptions at 1401 cm^{-1}. The resulting $\Delta\nu_{as-s}$ = ($\nu(CO_2)_{as}$–$\nu(CO_2)_s$) values of 184 cm^{-1} are consistent with monodentate bridging fashion of the carboxylate groups, according to the established correlation of $\Delta\nu_{as-s}$ with the coordination modes of carboxylate groups [21]. And sharp absorptions at 1104, 1068 cm^{-1} have been assigned to ν(C–OH) stretching vibration. It is thus clear that the FT-IR spectroscopic results of

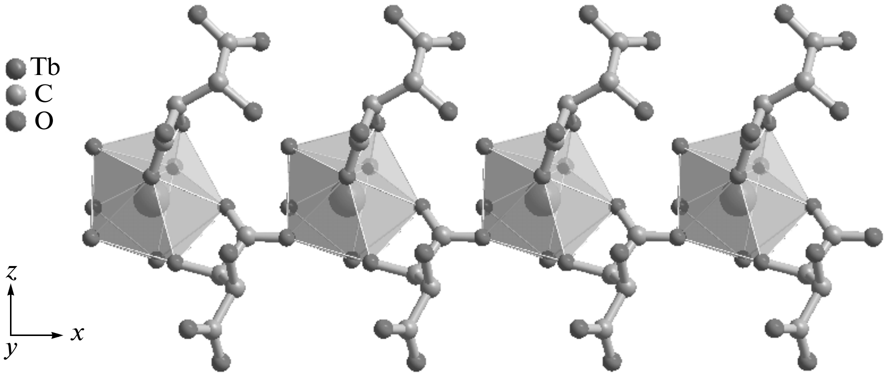

Fig. 2. 1D chain in the crystals of **I** along [100].

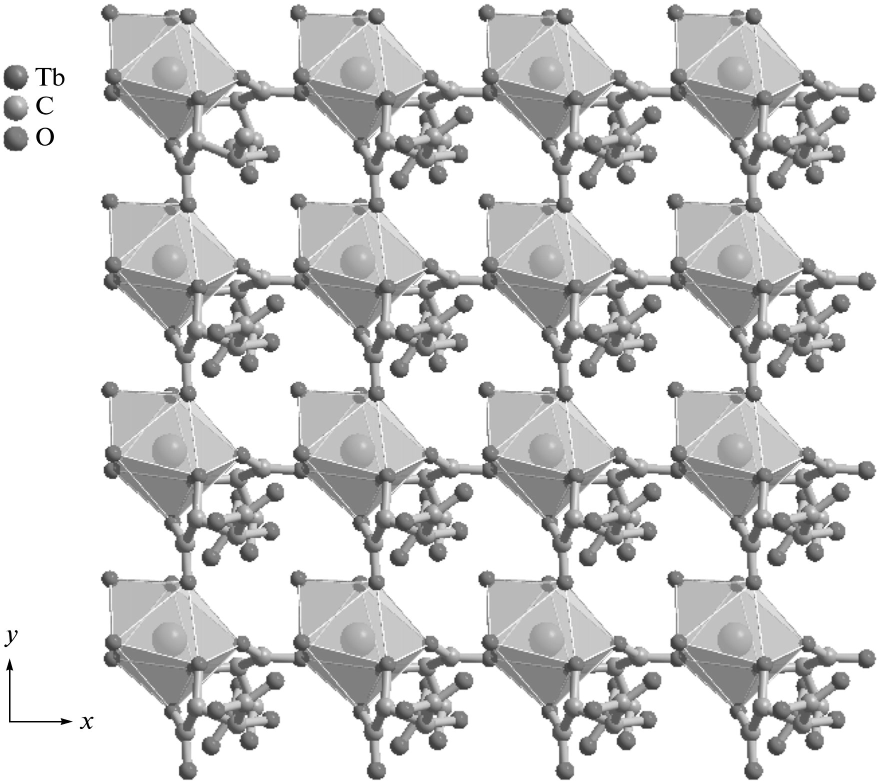

Fig. 3. A layer in the crystals of **I** parallel to the plane (001).

complex confirm the presence of tartrate ligands and establish that one of the tartrate ions is singly ionized.

The luminescent behaviors were investigated in the solid state at room temperature. As shown in Fig. 5, when excited at 353 nm, it emits green luminescence at room temperature. The characteristic luminescent bands of the terbium compound were recorded at 493, 548, 585, and 623 nm via ligand to metal energy transfer mechanism, which can be attributed to $^5D_4 \to {}^7F_J$ ($J = 6, 5, 4$, and 3) transitions, respectively. The spectrum is dominated by the $^5D_4 \to {}^7F_5$ transition, at 548 nm, which gives an intense green luminescence output for the solid sample.

It is well known that analysis of the magnetic interaction between rare-earth ions gives rise to additional difficulties since the magnitude of these interactions is comparable with that of the crystal field acting on the ion due to the large orbital contribution. The magnetic susceptibilities were measured in the temperature range from 2 to 300 K under 5 K Oe field, as shown in Fig. 6.

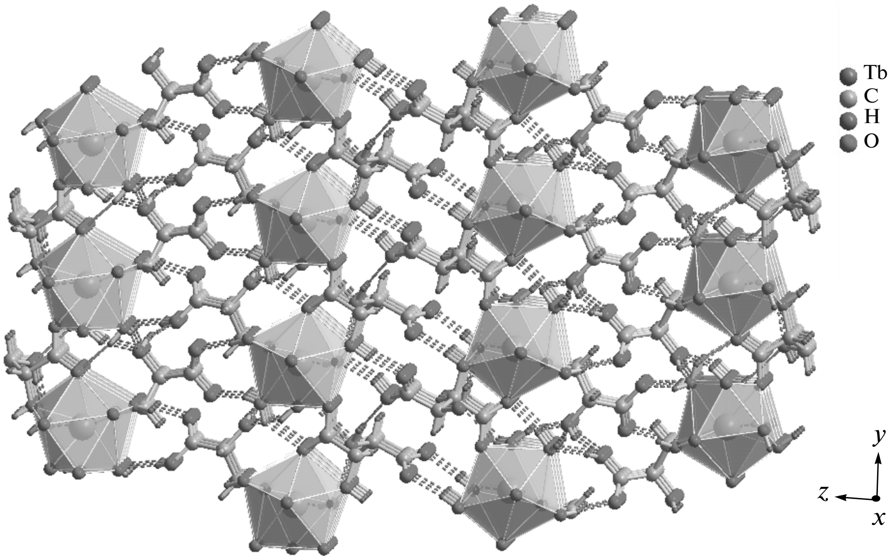

Fig. 4. A three-dimensional framework build by hydrogen bonds between layers.

The value of $\chi_M T$ at 300 K is 11.61 cm^3 K mol^{-1}, which is close to the theoretical value of 11.81 cm^3 K mol^{-1} expected for one Tb^{3+} ion in the $^7F_6$ ground state (g) 3/2. The $\chi_M T$ value slowly decreases on cooling and reaches a minimum value of 9.22 cm^3 K mol^{-1} at 2 K. On the basis of the reason mentioned above, we are not sure that antiferromagnetic coupling exists between adjacent Tb, because any weak exchange interaction within the structure is masked by crystal field effects. However, the plot of $\chi_M T$ vs T over the whole temperature range obeys the Curie–Weiss law [$\chi_M = C/(T-\theta)$] with $C = 15.31$ emu K mol^{-1} and $\theta = -1.23$ K. The increase of $\chi_M T$ within the higher temperature range coupled with the negative θ indicates a very weak antiferromagnetic coupling between Tb^{3+} ions.

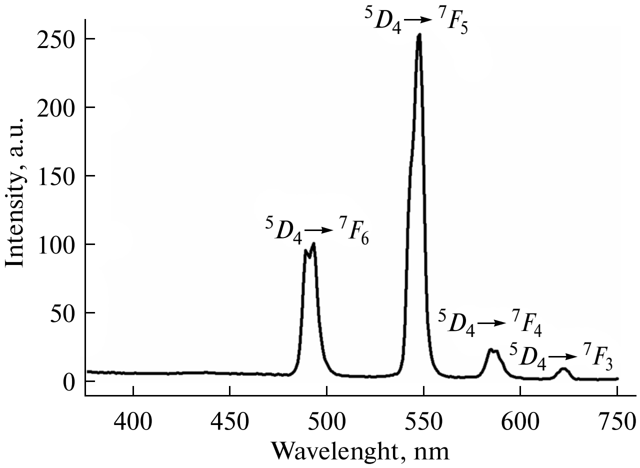

Fig. 5. Emission spectra of complex **I** in solid state at room temperature.

The powder second harmonic generation (SHG) was measured as described by Kurtz and Perry at $\lambda = 1064$ nm [22]. But no significant green light at a wavelength of 532 nm from powder sample was observed, maybe due to its extremely week SHG effect.

It is well known that acentric symmetry is a prerequisite for many technologically important properties such as ferroelectricity and second-order nonlinear optical behavior [23]. Given **I** crystallize in the acentrosymmetric space groups $P4_1$ with the point group C_4, which belongs to the 10 polar point groups (C_1, C_2, C_s, C_{2v}, C_3, C_{3v}, C_4, C_{4v}, C_6, C_{6v}) prerequisite for ferroelectricity, its ferroelectric properties were examined. Experimental results indicate that there exists an electric hysteresis loop that is a typical ferroelectric feature (Fig. 7). A remnant polarization $2P_r = 0.160$ C cm^{-2}, coercive field $2E_c = 44.5$ kV cm^{-1}, saturation of the spontaneous polarization $P_s = 0.176$ C cm^{-2}. The P_s value is slightly smaller than that of the typical ferroelectric compound Rochelle salt ($NaKC_4H_4O_6 \cdot 4H_2O$, $P_s = 0.25$ μC cm^{-2}) [24]. Therefore, complex **I** has a typical ferroelectric feature, which is corresponding to the acentric space group $P4_1$.

ACKNOWLEDGMENTS

This project was supported by the Scientific Research Fund of the Zhejiang Provincial Education

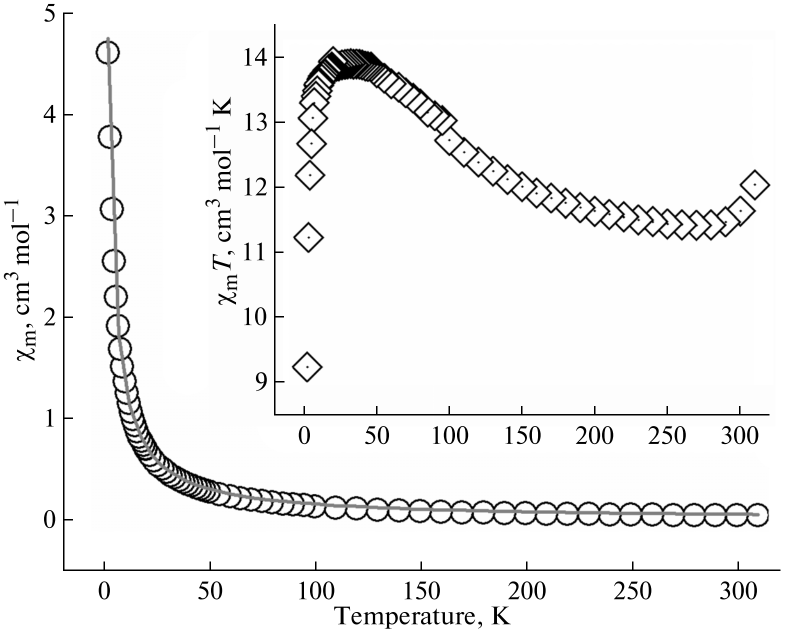

Fig. 6. Temperature dependence of the magnetic susceptibility of complex **I**.

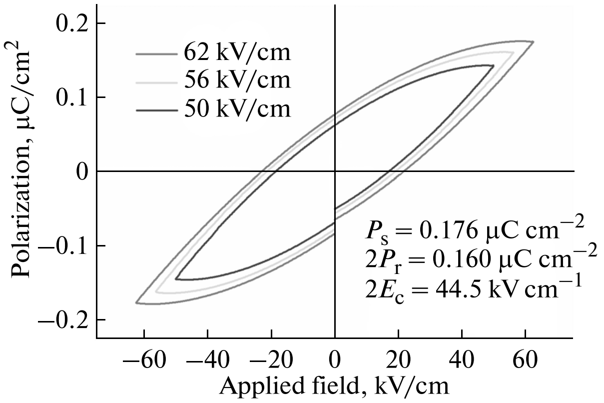

Fig. 7. Electric hysteresis loops of complex **I**, observed for powdered samples in the form of pellets on a ferroelectric tester at room temperature.

Department (grant no. Y201017782). The honest thanks are also extended to K.C. Wong Magna Fund of Ningbo University.

REFERENCES

1. Torres, M.E., Peraza, J., Yanes, A.C., et al., *J. Phys. Chem. Solids*, 2002, vol. 63, p. 491.
2. Fousek, J., Cross, L.E., and Seely, K., *Ferroelectrics*, 1970, vol. 1, p. 63.
3. Torres, M.E., Peraza, J., Yanes, A.C., et al., *J. Appl. Phys.*, 1998, vol. 84, p. 5729.
4. Medrano, C., Gunter, P., and Arend, H., *Phys. Status Solidi, B*, 1997, vol. 143, p. 749.
5. Watanabe, O., Noritake, T., Hirose, Y., et al., *J. Mater. Chem.*, 1993, vol. 3, p. 1053.
6. Zyss, J., Masse, R., Beucher-Bagieu, M., et al., *Adv. Mater.*, 1993, vol. 5, p. 120.
7. Ovchinnikova, G.I., Gavrilova, N.D., and Lotonov, A.M., *Izv. Akad. Nauk., Ser. Fiz.*, 1997, vol. 61, p. 2431.
8. Arora, S.K., Patel, V., Chudasama, B., et al., *J. Cryst. Growth*, 2005, vol. 275, p. e657.
9. Suryanarayana, K. and Dharmaprakash, S.M., *Mater. Lett.*, 2000, vol. 42, p. 92.
10. Arora, S.K., Patel, V., Kothari, A., et al., *Cryst. Growth. Des.*, 2004, vol. 4, p. 343.
11. Suryanarayana, K. and Dharmaprakash, S.M., *Mater. Chem. Phys.*, 2003, vol. 77, p. 179.
12. Tanase, S. and Reedijk, J., *Coord. Chem. Rev.*, 2006, vol. 250, p. 2501.
13. Handa, S., Nagawa, K., Sohtome, Y., et al., *Angew. Chem. Int. Ed.*, 2008, vol. 47, p. 3230.
14. Xia, J., Zhao, B., Wang, H.S., et al., *Inorg. Chem.*, 2007, vol. 46, p. 3450.
15. Manna, S.C., Zangrando, E., Ribas, J., et al., *Polyhedron*, 2006, vol. 25, p. 1779.
16. Athar, M., Li, G.H., Shi, Z., et al., *Solid State Sci.*, 2008, vol. 10, p. 1853.
17. Yan, P., Xing, J.C., Li, G.M., et al., *J. Coord. Chem.*, 2009, vol. 62, p. 2095.
18. Sheldrick, G.M., *SHELXS-97, Program for Crystal Stucture Refinement and SHELXL-97, Program for Crystal Stucture Solution*, Göttingen (Germany): Univ. of Göttingen, 1997.
19. Wu, C.D., Zhan, X.P., Lu, C.Z., et al., *Acta Crystallogr., E*, 2002, vol. 58, p. m228.
20. Hawrhorne, F.C., Borys, I., and Ferguson, R.B., *Acta Crystallogr., C*, 1983, vol. 39, p. 540.
21. Nakamoto, K., *Infrared and Raman Spectra of Inorganic and Coordination Compounds*, Pt. B, New York: Interscience-Wiley, 2009.
22. Perry, T.T. and Kurtz, S.K., *J. Appl. Phys.*, 1968, vol. 39, p. 3798.
23. Halasyamani, P.S. and Poeppelmeier, K.R., *Chem. Mater.*, 1998, vol. 10, p. 2753.
24. Solans, X., Gonzalez-Silgo, C., and Ruiz-Pérez, C., *J. Solid State Chem.*, 1997, vol. 131, p. 350.